



## CHEMICAL ANALYSIS OF A CARBON-ENHANCED VERY METAL-POOR STAR: CD-27 14351

DRISYA KARINKUZZHI<sup>1</sup>, ARUNA GOSWAMI<sup>1</sup>, AND THOMAS MASSERON<sup>2</sup>

<sup>1</sup>Indian Institute of Astrophysics, Koramangala, Bangalore 560034, India

<sup>2</sup>Institute of Astronomy, Madingley Road, Cambridge CB3 0HA, UK

Received 2016 September 19; revised 2016 October 31; accepted 2016 October 31; published 2017 January 3

### ABSTRACT

We present, for the first time, an abundance analysis of a very metal-poor carbon-enhanced star CD-27 14351 based on a high-resolution ( $R \sim 48,000$ ) FEROS spectrum. Our abundance analysis performed using local thermodynamic equilibrium model atmospheres shows that the object is a cool star with stellar atmospheric parameters, effective temperature  $T_{\text{eff}} = 4335$  K, surface gravity  $\log g = 0.5$ , microturbulence  $\xi = 2.42$  km s<sup>-1</sup>, and metallicity  $[\text{Fe}/\text{H}] = -2.6$ . The star exhibits high carbon and nitrogen abundances with  $[\text{C}/\text{Fe}] = 2.89$  and  $[\text{N}/\text{Fe}] = 1.89$ . Overabundances of neutron-capture elements are evident in Ba, La, Ce, and Nd, with estimated  $[\text{X}/\text{Fe}] > 1$ , the largest enhancement being seen in Ce with  $[\text{Ce}/\text{Fe}] = 2.63$ . While the first peak *s*-process elements Sr and Y are found to be enhanced with respect to Fe, ( $[\text{Sr}/\text{Fe}] = 1.73$  and  $[\text{Y}/\text{Fe}] = 1.91$ ), the third peak *s*-process element Pb could not be detected in our spectrum at the given resolution. Europium, primarily an *r*-process element also shows an enhancement with  $[\text{Eu}/\text{Fe}] = 1.65$ . With  $[\text{Ba}/\text{Eu}] = 0.12$ , the object CD-27 14351 satisfies the classification criterion for a CEMP-*r/s* star. The elemental abundance distributions observed in this star are discussed in light of the chemical abundances observed in other CEMP stars in the literature.

*Key words:* stars: carbon – stars: chemically peculiar – stars: late-type – stars: low-mass

### 1. INTRODUCTION

The object CD-27 14351 drew our attention when a low-resolution spectrum of this object acquired on 2015 October 23, during the observing run of our observational program with HCT (Himalayan *Chandra* Telescope, at Indian Astronomical Observatory (IAO), Hanle; one of the objectives of this program is to search for CH stars and carbon-enhanced metal-poor stars among field stars) on visual inspection was found to show significant resemblance to the low-resolution spectrum of HD 5223, a well known classical CH star. From the known stellar parameters of HD 5223, ( $T_{\text{eff}} = 4500$  K,  $\log g = 1.0$ , and metallicity  $[\text{Fe}/\text{H}] = -2.06$  (Goswami et al. 2006), a first guess was that the object CD-27 14351 could be a cool metal-poor object similar to HD 5223. Dominant carbon-bearing molecular bands in its spectrum also indicated that the object is likely carbon-enhanced. For an understanding of its elemental abundance pattern and its origin, a detailed chemical composition study was undertaken based on a high-resolution FEROS (Fiber-fed Extended Range Optical Spectrograph, connected to the 1.52 m telescope in Chile) spectrum.

Our analysis reveals that the object is indeed a carbon-enhanced metal-poor star that also shows significant enhancement of nitrogen and neutron-capture elements. The heavy elements abundance estimates indicate that the surface composition of the object has significant contributions that originated from both the *r*-process as well as the *s*-process nucleosynthesis. This is supported by our estimate of the abundance ratio  $[\text{Ba}/\text{Eu}] (=0.12)$ , that qualifies the object to be placed in the CEMP-*r/s* group (Beers & Christlieb 2005, for a definition of CEMP-*r/s* stars and other CEMP stars). However, the origin of CEMP-*r/s* stars is still far from being clearly understood. Several proposed physical scenarios are available in the literature (Qian & Wasserburg 2003; Nomoto et al. 2004; Zijlstra 2004; Barbuy et al. 2005; Wanajo et al. 2006). In spite of considerable effort, no single mechanism has yet been identified that could explain satisfactorily the production of enhanced carbon and heavy-element abundance patterns

observed in this group of stars. While the enhancement in the *s*-process elements is believed to be due to mass transfer in binary systems involving an asymptotic giant branch companion that underwent *s*-process nucleosynthesis, the origin of the enhanced abundance of the *r*-process element Eu remains unexplained in this scenario. In a recent work, Hampel et al. (2016) showed that the observed abundance patterns of CEMP-*r/s* stars could be convincingly reproduced through *i*-process (intermediate neutron-capture process), which operates at neutron densities between those of the *s*-process and *r*-process. Except for one object, the abundance patterns of all the stars in their sample could be reproduced by this process. To place observational constraints on the nucleosynthesis of *s*-, *r*-, and *i*-process elements at low metallicity, it is necessary to conduct high-resolution spectroscopic analysis of stars with an excess of heavy elements, and CEMP stars undoubtedly form important targets. Such studies would help provide insight into the possible origin of this class of objects. Our detailed high-resolution spectroscopic analysis of CD-27 14351 is prompted by such motivation.

In Section 2, we describe the source of the low-resolution and high-resolution spectra of the program star. In Section 3, we present our estimates of effective temperatures based on available BVJHK photometry of the object. The spectral analysis procedures and estimation of the stellar atmospheric parameters are discussed in Section 4. The elemental abundance results and discussions are presented in Section 5. Uncertainty in elemental abundances is discussed in Section 6. Conclusions are provided in Section 7.

### 2. SPECTRA OF CD-27 14351

The low-resolution spectrum of CD-27 14351 was acquired on 2015 October 23, using HFOSC attached to the 2 m HCT (Himalayan *Chandra* Telescope) at the IAO, Mt Saraswati, Digpa-ratsa Ri, Hanle. The spectrograph used is HFOSC (Himalayan Faint Object Spectrograph Camera). The spectrum covers the wavelength range 3800–6800 Å at a resolution of

**Table 1**  
Basic Data for the Program Stars

Star Name	R.A.(2000)	Decl.(2000)	B	V	J	H	K
CD-27 14351	19 53 08.00	-27 28 14.96	11.82	9.70	7.022	6.296	6.135

**Table 2**  
Temperatures from Photometry

Star Name	$T_{\text{eff}}$ (J-K) K	$T_{\text{eff}}$ (J-H) K	$T_{\text{eff}}$ (V-K) K	$T_{\text{eff}}$ (B-V) K	Spectroscopic K
CD-27 14351	4067	4026 (-2.0)	3900 (-2.0)	2635(-2.0)	4335
		3989(-2.5)	3900 (-2.5)	2528(-2.5)	
		3938(-3.0)	3904 (-3.0)	2438(-3.0)	

**Note.** The numbers in parenthesis indicate the metallicity values at which the temperatures are calculated.

$R \sim 1300$ . The high-resolution FEROS (FEROS: the Fiber-fed Extended Range Optical Spectrograph, connected to the 1.52 m telescope at ESO, Chile) spectrum of CD-27 14351 used in this study was acquired on 2000 July 14, has a resolution of  $R \sim 48,000$ , and covers the wavelength range spanning 3500–9000 Å. The estimated radial velocity is  $\sim 61.1 \text{ km s}^{-1}$ . The basic data for this object are listed in Table 1.

### 3. TEMPERATURES FROM PHOTOMETRIC DATA

We have calculated the photometric temperatures of CD-27 14351 using the temperature calibrations of Alonso et al. (1999, 2001) for the giants. The estimated values along with the spectroscopic temperature estimate are given in Table 2. As can be seen in the following section, the derived spectroscopic temperatures are higher by  $\approx 300 \text{ K}$  from J–K and J–H temperatures, and  $\approx 400 \text{ K}$  from the V–K temperatures. This discrepancy is probably due to the high carbon enhancement that significantly changes the colors; due to the severe blending from the molecular lines, B–V temperatures could be much lower than the spectroscopic temperature estimate.

### 4. SPECTRAL ANALYSIS

In Figure 1, we show a comparison of the spectrum of CD-27 14351 with the spectrum of the classical CH star HD 5223 (Goswami 2005) obtained from the same observational setup. The spectra of these two objects distinctly show a close resemblance to each other. The high-resolution FEROS spectrum is used for determination of stellar atmospheric parameters and elemental abundances. The stellar parameters are determined by measuring the equivalent widths of clean unblended Fe I and Fe II lines. The spectrum of CD-27 14351 is severely blended with contributions from carbon molecular bands throughout the spectrum, making it difficult to find clean unblended lines of Fe I and Fe II. Only seventeen lines of Fe I and two lines of Fe II are found usable for deriving the stellar atmospheric parameters. Lines with excitation potential in the range 0.0–5.0 eV and equivalent width 20–160 Å are selected for this purpose. These lines, along with the abundances derived from each line computed using the latest version of MOOG (Snedden 1973), are listed in Table 3. We have used the Kurucz grid of model atmospheres with no convective overshooting (<http://cfaku5.cfa.harvard.edu/>) and assumed a local thermodynamic equilibrium (LTE) condition throughout the analysis. The method of excitation equilibrium is used for

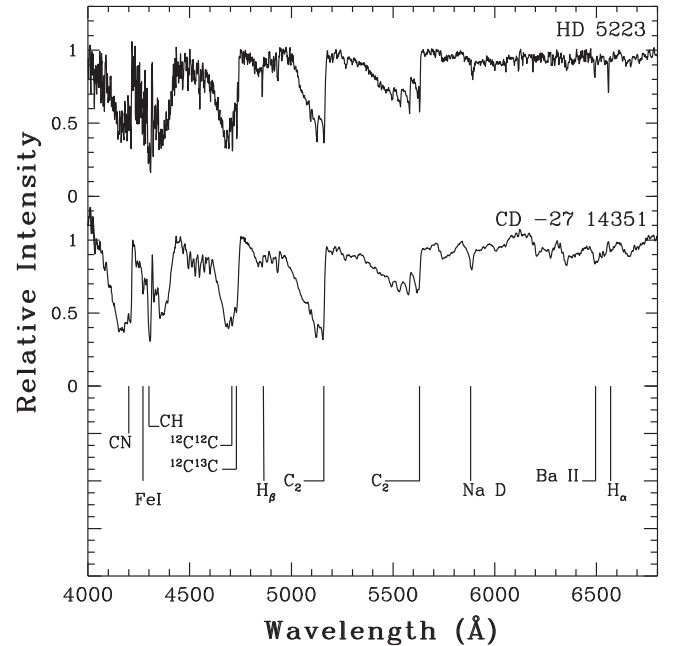


**Figure 1.** A comparison of the low-resolution spectrum of CD-27 14351 with the spectrum of CH star HD 5223. Some prominent features are indicated in the figure.

deriving the effective temperature  $T_{\text{eff}}$ . The initial value is assumed to be the photometric temperatures and the finally adopted value is obtained by an iterative process until the slope of the abundance versus excitation potential of Fe I lines is found to be nearly zero (Figure 2, lower panel). The microturbulent velocity is fixed at this temperature by demanding that there be no dependence of the derived Fe I abundance on the equivalent widths of the corresponding lines (Figure 2, upper panel). The surface gravity is fixed at a value that makes the abundances of iron from the Fe I and Fe II lines equal. The adopted stellar parameters are listed in Table 4.

### 5. RESULTS AND DISCUSSIONS: ELEMENTAL ABUNDANCES

Elemental abundances are derived from the measured equivalent widths of lines due to neutral and ionized elements if clean unblended lines are present. We have also performed spectral-synthesis calculations to derive the elemental abundances for a few elements considering the hyperfine splitting effects. These elemental abundances along with the abundance

**Table 3**  
Lines Used for the Analysis

Wavelength (Å)	Element	$E_{\text{low}}$ (ev)	$\log gf$	Equivalent Width (mÅ)	$\log \epsilon$ (dex)	Reference
5688.220	Na I	2.104	-0.45	58.3	4.89	(1)
4571.100	Mg I	0.000	-5.69	154.1	5.88	(2)
5528.405		4.350	-0.62	61.1	5.04	(3)
5172.680		2.710	-0.40	304.7	5.92	(4)
5261.710	Ca I	2.521	-0.73	27.1	4.39	(5)
6439.070		2.530	0.47	109.6	4.42	(5)
6499.650		2.523	-0.59	65.2	4.72	(5)
4999.500	Ti I	0.830	0.25	134.0	3.33	(6)
5210.390		0.048	-0.88	120.6	3.04	(6)
5192.970		0.020	-1.01	143.1	3.38	(6)
4443.790	Ti II	1.080	-0.70	178.7	3.29	(6)
4589.950		1.236	-1.79	94.9	3.02	(6)
5226.530		1.570	-1.30	131.9	3.30	(6)
5247.570	Cr I	0.961	-1.64	29.0	2.95	(6)
5348.312		1.003	-1.29	33.0	2.72	(6)
4476.019	Fe I	2.845	-0.57	108.1	4.98	(7)
4890.755		2.876	-0.43	121.2	4.68	(8)
4924.770		2.279	-2.22	79.4	5.16	(8)
4982.524		4.103	0.14	66.9	4.99	(9)
4994.130		0.915	-3.08	149.7	5.06	(8)
5171.600		1.485	-1.79	160.5	4.69	(8)
5194.941		1.557	-2.09	148.5	4.89	(8)
5198.711		2.223	-2.14	73.1	4.85	(8)
5202.340		2.180	-1.84	122.2	5.12	(8)
5217.389		3.211	-1.10	69.2	5.07	(9)
5247.050		0.087	-4.98	83.3	4.84	(8)
5307.370		1.610	-2.98	69.4	4.74	(8)
5339.928		3.266	-0.68	68.1	4.70	(8)
5415.192		4.386	0.50	60.9	4.73	(8)
6137.694		2.588	-1.40	98.0	4.77	(8)
6136.615		2.453	-1.40	114.4	4.78	(8)
6421.350		2.278	-2.03	92.8	4.90	(8)
5234.625	Fe II	3.22	-2.05	38.5	4.97	(8)
5276.002		3.199	-1.90	40.5	4.88	(8)
4607.327 <sup>a</sup>	Sr I	0.000	-0.57	43.9	2.02	(10)
5289.815 <sup>a</sup>	Y II	1.033	-1.85	70.4	1.52	(11)
5662.925		1.944	0.16	135.5	1.74	(12)
4934.076	Ba II	0.000	-0.15	414.6	1.38	(5)
6141.713 <sup>a</sup>		0.704	-0.08	287.2	1.34	(5)
6496.897		0.604	-0.38	298.0	1.47	(5)
4526.111	La II	0.772	-0.77	60.1	0.49	(13)
4921.776 <sup>a</sup>		0.244	-0.68	94.6	0.09	(14)
4460.207	Ce II	0.477	0.17	146.3	1.49	(15)
4527.348		0.320	-0.46	144.3	1.79	(15)
4451.981	Nd II	0.000	-1.34	38.3	0.10	(16)
4811.342		0.063	-1.14	50.9	0.07	(16)
5212.361 <sup>a</sup>		0.204	-0.87	61.5	0.04	(16)
5293.163		0.823	-0.00	71.7	0.22	(17)
6645.064 <sup>a</sup>	Eu II	1.380	0.20	synth	-0.40	(18)

#### Notes.

(1) Kurucz & Peytreman (1975), (2) Laughlin & Victor (1974), (3) Lincke & Ziegenbein (1971), (4) Anderson et al. (1967), (5) Miles & Wiese (1969), (6) Martin et al. (1988), (7) Bridges & Kornblith (1974), (8) Führ et al. (1988), (9) Kurucz (1988), (10) Corliss & Bozman (1962b), (11) Hannaford et al. (1982), (12) Cowley & Corliss (1983), (13) Andersen et al. (1975), (14) Corliss & Bozman (1962a) adjusted, (15) McEachran & Cohen (1971), (16) Meggers et al. (1975) adjusted, (17) Ward et al. (1985), (18) Biemont et al. (1982).

<sup>a</sup> Abundances are also derived by spectral-synthesis calculations of these lines. The results are presented in Table 5.

ratios with respect to iron are presented in Table 5. We have also calculated the [ls/Fe], [hs/Fe] and [hs/lis] values, where ls represents light *s*-process elements Sr and Y, and hs represents heavy *s*-process elements Ba, La, Ce, and Nd. These estimates are presented in Table 6.

#### 5.1. Carbon, Nitrogen, Oxygen

Several strong molecular features of carbon are clearly noticeable throughout the spectrum of CD-27 14351. We have calculated the carbon abundance from the spectral synthesis of the C<sub>2</sub> band at 5635 Å (Figure 3, middle panel). The C<sub>2</sub> band at

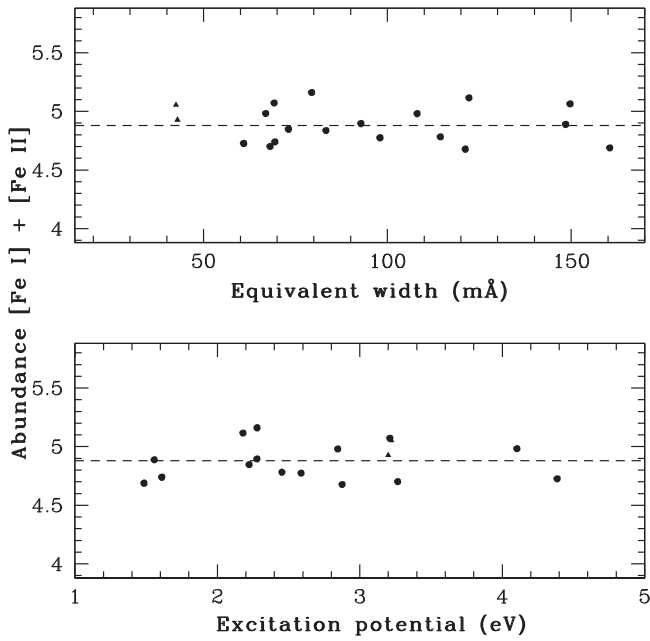


**Figure 2.** The iron abundance of CD-27 14351 is shown for individual Fe I (solid circles) and Fe II (solid triangles) lines as a function of excitation potential (lower panel) and as a function of equivalent width (upper panel).

**Table 4**  
Derived Atmospheric Parameters of CD-27 14351

Star Name	$T_{\text{eff}}$ (K)	$\log g$	$\xi$ ( $\text{km s}^{-1}$ )	[Fe I/H]	[Fe II/H]
CD-27 1435	4335	0.5	2.42	-2.62	-2.57

**Table 5**  
Elemental Abundances in CD-27 14351

	Z	Solar $\log \epsilon^a$	$\log \epsilon$	[X/H]	[X/Fe]
C I	6	8.43	$8.70 \pm 0.20$	0.27	2.89
N I	7	7.83	$7.10 \pm 0.20$	-0.73	1.89
Na I	11	6.24	$4.89 \pm 0.20$	-1.35	1.27
Mg I	12	7.60	$5.61 \pm 0.40$	-1.99	0.63
Ca I	20	6.34	$4.51 \pm 0.18$	-1.83	0.79
Ti I	22	4.95	$3.25 \pm 0.18$	-1.70	0.92
Ti II	22	4.95	$3.21 \pm 0.16$	-1.74	0.83
Cr I	24	5.64	$2.84 \pm 0.17$	-2.80	-0.18
Fe I	26	7.50	$4.87 \pm 0.15$	-2.63	...
Fe II	26	7.50	$4.93 \pm 0.09$	-2.57	...
Sr I	38	2.87	$2.02 \pm 0.20$	-0.85	1.77
Sr I <sup>b</sup>	38	2.87	$1.98 \pm 0.20$	-0.89	1.73
Y II	39	2.21	$1.63 \pm 0.12$	-0.58	1.99
Y II <sup>b</sup>	39	2.21	$1.55 \pm 0.20$	-0.66	1.91
Ba II	56	2.18	$1.40 \pm 0.07$	-0.78	1.79
Ba II <sup>b</sup>	56	2.18	$1.38 \pm 0.20$	-0.8	1.77
La II	57	1.10	$0.29 \pm 0.18$	-0.81	1.76
La II <sup>b</sup>	57	1.10	$0.10 \pm 0.20$	-1.00	1.57
Ce II	58	1.58	$1.43 \pm 0.30$	-0.15	2.63
Nd II	60	1.42	$0.11 \pm 0.08$	-1.31	1.26
Nd II <sup>b</sup>	60	1.42	$-0.05 \pm 0.20$	-1.47	1.10
Eu II <sup>b</sup>	63	0.52	$-0.40 \pm 0.20$	-0.92	1.65

**Notes.**

<sup>a</sup> Asplund et al. (2009).

<sup>b</sup> Abundance estimates are from spectral-synthesis calculation.

**Table 6**  
Abundance Ratios of Light and Heavy *s*-process Elements

Star Name	[Fe/H]	[ls/Fe]	[hs/Fe]	[hs/ls]
CD-27 14351	-2.62	1.82	1.77	-0.05

**Note.** [ls/Fe] and [hs/Fe] are calculated using the abundance values obtained from spectral-synthesis calculations, as given in Table 5.

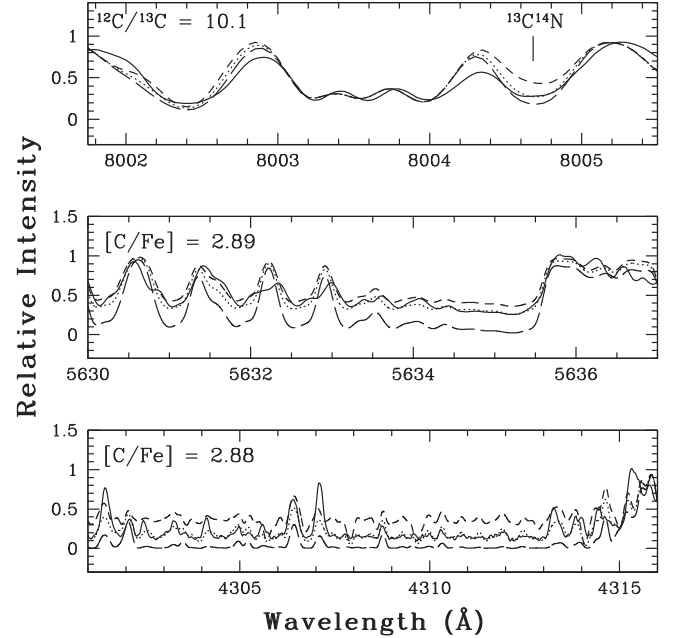


**Figure 3.** Lower panel: the spectral-synthesis fits of the CH feature around 4315 Å. Middle panel: the spectral synthesis of the  $\text{C}_2$  band around 5635 Å. In both the panels, the dotted lines indicate the synthesized spectra and the solid lines indicate the observed line profiles. Two alternative synthetic spectra for  $[\text{C}/\text{Fe}] = +0.3$  (long-dashed line) and  $[\text{C}/\text{Fe}] = -0.3$  (short-dashed line) are shown to demonstrate the sensitivity of the line strength to the abundances. Top panel: the spectral-synthesis fits of the CN features around 8005 Å obtained with the adopted N abundance and  $^{12}\text{C}/^{13}\text{C} \sim 10.1$  (dotted curve). The observed spectrum is shown by a solid curve. Two alternative fits with  $^{12}\text{C}/^{13}\text{C} \sim 25$  (short-dashed line) and 5 (long-dashed line) are shown to illustrate the sensitivity of the line strengths to the isotopic carbon abundance ratios.

5165 Å is found to be saturated. Carbon shows a large enhancement with  $[\text{C}/\text{Fe}]$  value of 2.89 as estimated from the  $\text{C}_2$  molecular band at 5635 Å. The abundance of carbon derived from the CH band at 4300 Å (Figure 3, lower panel) also shows similar value with  $[\text{C}/\text{Fe}] = 2.88$ . For the line lists of CH,  $\text{C}_2$ , CN, and  $^{12}\text{C}/^{13}\text{C}$  we have consulted Masseron et al. (2014), Brooke et al. (2013), Sneden et al. (2014), and Ram et al. (2014). Using the estimated carbon abundance, the nitrogen abundance was derived from the spectral-synthesis calculation of the CN band with the band head at 4215 Å (Figure 4). The estimated nitrogen abundance  $\sim 7.1$  dex gives  $[\text{C}/\text{N}] = 1.0$  for this object. We could not detect any oxygen lines in the spectrum due to severe distortion in the spectrum. We have estimated the  $^{12}\text{C}/^{13}\text{C}$  ratio from the  $^{12}\text{CN}$  and  $^{13}\text{CN}$  features near 8005 Å (Figure 3, top panel). We have estimated  $^{12}\text{C}/^{13}\text{C} = 10.1$  for this object. Such a low value is not unreasonable as the estimated  $\log g$  value of CD-27 14351 indicates that the object is an evolved red giant star in which

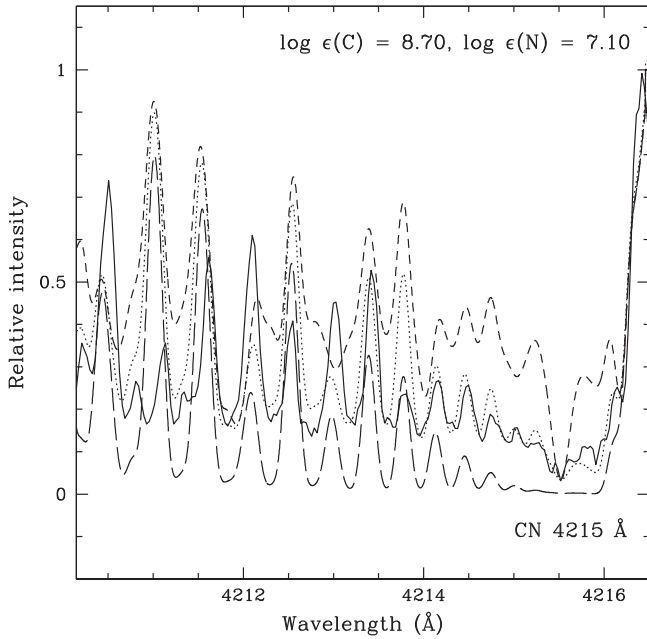


**Figure 4.** Spectral-synthesis fits of the CN band around 4215 Å. The best fit obtained with a carbon abundance of 8.7 dex and  $^{12}\text{C}/^{13}\text{C} \sim 10.1$  returns a nitrogen abundance of 7.1 dex (dotted lines). The solid line corresponds to the observed spectrum. Two alternative plots with long-dash and short-dash are shown with  $[\text{N}/\text{Fe}] = \pm 0.3$  from the adopted value.

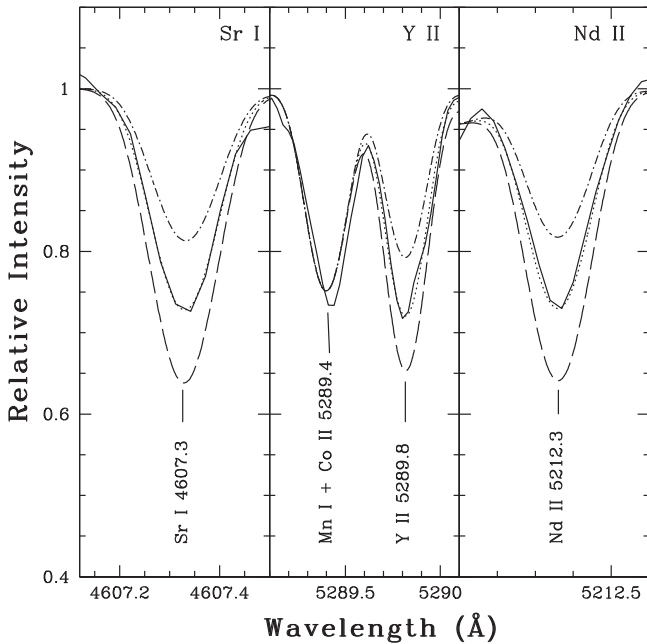


**Figure 5.** Spectral-synthesis fits of the Sr I line at 4607.3 Å, Y II line at 5289.8 Å, and Nd II line at 5212.3 Å are shown. The dotted lines indicate the synthesized spectra and the solid lines indicate the observed line profiles. Two alternative synthetic spectra for  $[\text{X}/\text{Fe}] = +0.3$  (long-dashed line) and  $[\text{X}/\text{Fe}] = -0.3$  (short-dashed line) from the adopted value are shown to demonstrate the sensitivity of the line strength to the abundances.

the CN cycled materials are expected to mix together into the atmosphere, making the  $^{12}\text{C}/^{13}\text{C}$  ratio low.

### 5.2. Sodium (Na) and Aluminum (Al)

We have derived the Na abundance from the Na I line at 5688.22 Å. The estimated Na abundance is high with  $[\text{Na}/\text{Fe}]$

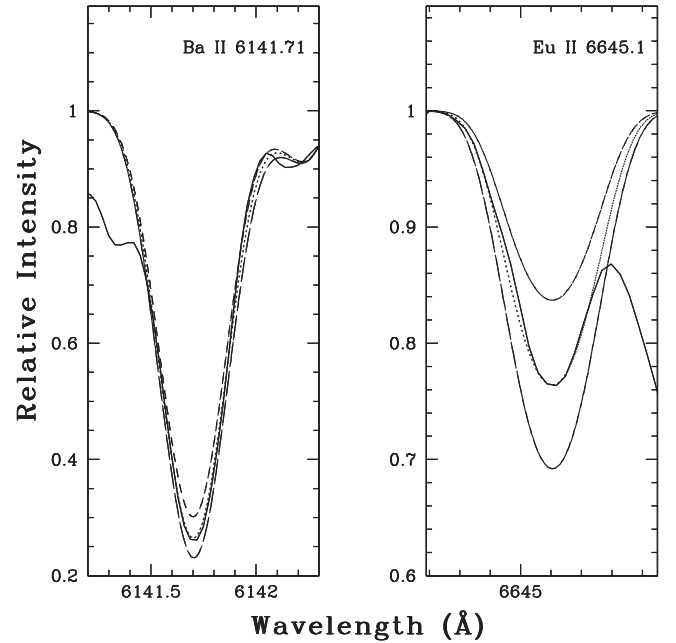


**Figure 6.** Spectral-synthesis fits of the Ba II line at 6141.71 Å and Eu II line at 6645 Å. In both the panels, the dotted lines indicate the synthesized spectra and the solid lines indicate the observed line profiles. Two alternative synthetic spectra for  $[\text{X}/\text{Fe}] = +0.3$  (long-dashed line) and  $[\text{X}/\text{Fe}] = -0.3$  (short-dashed line) from the adopted value are shown to demonstrate the sensitivity of the line strength to the abundances.

$= 1.27$ . Since this line is free from NLTE effects (Baumueller & Gehren 1997), we have not applied NLTE correction to the derived abundance. A few very metal-poor stars are also known to show such high abundances of Na (Aoki et al. 2002a, 2002b, 2007, 2008). The abundance of Al could not be estimated in CD-27 14351.

### 5.3. Abundances of $\alpha$ -elements

We have estimated  $[\text{Mg}/\text{Fe}] \sim 0.64$  from three Mg I lines at 4571.1, 5172.68, and 5528.41 Å. This value is slightly higher than the general trend of  $[\alpha/\text{Fe}] = 0.4$  noticed in metal-poor stars. We have measured three clean Ca I lines in the spectrum of CD-27 14351. Similar to Mg, Ca also shows large enhancement with a  $[\text{Ca}/\text{Fe}]$  value of 0.79. Ti shows enhancement with  $[\text{Ti I}/\text{Fe}]$  and  $[\text{Ti II}/\text{Fe}]$  values of 0.92 and 0.83, respectively. Johnson (2002) has also found that Ti I and Ti II are discrepant in metal-poor stars, likely because of NLTE effects. These estimates show that the object is a very metal-poor star with high abundances of  $\alpha$  elements.

### 5.4. Fe-peak Elements

Two Cr I lines at 5247.57 and 5348.31 Å are used to derive the Cr abundance. Cr shows underabundance with a  $[\text{Cr}/\text{Fe}]$  value  $-0.18$ . We have detected many Ni lines in the spectrum of CD-27 14351. But none of them are usable for abundance calculation due to distortion and severe line blending.

### 5.5. Abundances of Neutron-capture Elements

Abundances of neutron-capture elements are derived by the equivalent width measurements as well as spectral-synthesis calculations. We have accounted for any possible blending due to other elements in the line lists of the respective lines used for

**Table 7**  
Abundance Uncertainties

Star	Standard Error	$\delta T_{\text{eff}}$ $\pm 100$ K	$\delta \log g$ $\pm 0.1$	$\delta \xi$ $\pm 0.3 \text{ km s}^{-1}$	Total Uncertainty
CD-27 14351	0.15	0.08	0.01	0.09	0.17

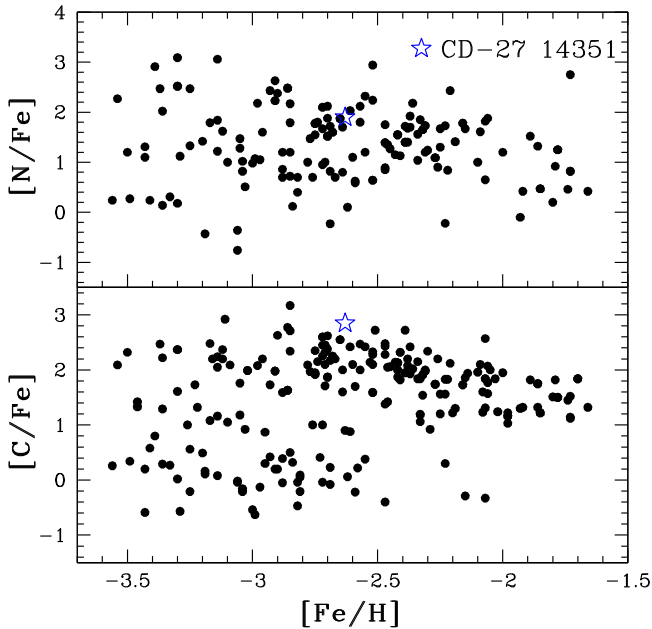


**Figure 7.** This figure shows a comparison of the  $[C/Fe]$  (lower panel) and  $[N/Fe]$  (upper panel) values observed in CD-27 14351 (shown with a star symbol in both the panels) with their counterparts (solid circles) in CEMP stars from the literature (e.g., Masseron et al. 2010).

spectral-synthesis calculation. The derived abundances along with the error estimates are listed in Table 5. The abundance of Sr is derived from the Sr I line at 4607.7 Å. Sr is found to be enhanced with  $[Sr/Fe] \sim 1.75$ . Y also shows an enhancement with  $[Y/Fe] \sim 1.95$ . The spectrum synthesis fits are shown in Figure 5. We could not measure any Zr lines in the spectrum of CD-27 14351. Ba abundance calculated by measuring the equivalent widths of Ba II lines at 4934, 6141, and 6496 Å give a  $[Ba/Fe]$  value of 1.79. The spectrum synthesis of the Ba II line at 6141.713 Å (Figure 6), considering the hyperfine splitting contributions from McWilliam (1998), gives  $[Ba/Fe] \sim 1.77$ . We have derived La abundance from the spectrum synthesis calculation of the La II line at 4921.77 Å, considering hyperfine components from Jonsell et al. (2006), which gives  $[La/Fe] \sim 1.57$ . Cerium abundance derived from two Ce II lines at 4460.2 and 4527.3 Å indicates a large enhancement of Ce with  $[Ce/Fe] \sim 2.63$ . Nd abundance calculated by the equivalent width measurement of four Nd II lines gives  $[Nd/Fe] \sim 1.26$ . We have also derived the Nd abundance by spectral-synthesis calculation of the Nd II line at 5212.3 Å (Figure 5); this gives a value of 1.1 for  $[Nd/Fe]$ . We have derived Eu abundance from the Eu II line at 6645.130 Å by considering the hyperfine components from Worley et al. (2013). Although the right wing of this Eu line is found to be blended with the Fe I line at 6645.36 Å and a Tb I line at 6645.37 Å, we could get a proper fit for the left wing with the adopted Eu abundance of  $-0.40$  dex (Figure 6). The adopted

Eu abundance gives  $[Eu/Fe] \sim 1.65$ . We could not detect Eu lines at 4129 and 6437 Å.

## 6. UNCERTAINTY IN ELEMENTAL ABUNDANCE

We have derived the uncertainties in elemental abundance estimates by varying the stellar atmospheric parameters  $T_{\text{eff}}$ ,  $\log g$ , and microturbulence in the model atmosphere. We have calculated the uncertainty due to temperature by varying the temperatures by  $\pm 100$  K and recalculated the Fe abundance. Similarly, by varying the  $\log g$  value by  $\pm 0.1$  and microturbulent velocity by  $\pm 0.1 \text{ km s}^{-1}$ , we have calculated the corresponding uncertainties in abundances due to these changes. These values, along with the standard error are listed in Table 7. The total uncertainty is calculated using the standard equation of error calculations

$$E_r = \sqrt{E_{r1}^2 + E_{r2}^2 + E_{r3}^2 + E_{r4}^2}. \quad (1)$$

We have assumed this value as the minimum error in the derived abundances.

## 7. CONCLUSIONS

A detailed chemical composition study of CD-27 14351 based on a high-resolution FEROS spectrum revealed many important features of this object. The object is characterized by a large enhancement in carbon; a similar enhancement in nitrogen is also evident from our analysis. Such high abundances of carbon and nitrogen are also seen in other CEMP stars (Figure 7); these two elements, however, show a large scatter with respect to metallicity. The  $\alpha$ -elements Mg, Ca, Ti, and Fe-peak element Cr show similar abundances to those generally noticed in CEMP stars; the high abundance of Na is also a common feature of many CEMP stars (Figure 8). A comparison of our estimated abundance ratios of neutron-capture elements with those of Allen et al. (2012), 2016 Goswami et al. (2006; 2016 Goswami & Aoki 2010), and Masseron et al. (2010), for CEMP stars, is shown in Figure 9. A similar comparison of the neutron-capture elements abundance ratios observed in CD-27 14351 with their counterparts observed in CEMP-s and CEMP-r/s stars alone from Jonsell et al. (2006) clearly shows that Sr, Y, and Ce are highly enhanced, whereas Ba, La, and Eu are similarly enhanced, as can be seen in the case of CEMP-r/s stars (Figure 10). Large enhancement of  $s$ -process elements along with the enhancement in Mg indicates the operation of  $^{22}\text{Ne}(\alpha, n)^{25}\text{Mg}$  as the main neutron source in CEMP-r/s stars (Masseron et al. 2010). As suggested by Gallino et al. (1998) and Goriely & Mowlavi (2000), neutron density associated with this reaction favors the production of the  $s$ -process element Ce and also the  $r$ -process element Eu. Highly enhanced abundances of these two elements observed in this star support this idea. However, Goriely & Siess (2005) suggest that a  $-ve$  value of  $[La/Ce]$  indicates the operation of  $^{13}\text{C}(\alpha, n)^{16}\text{O}$  reaction, and, a value of  $[La/Ce]$  within the range 0.2–0.4 indicates the operation of  $^{22}\text{Ne}(\alpha, n)^{25}\text{Mg}$  reaction. Our

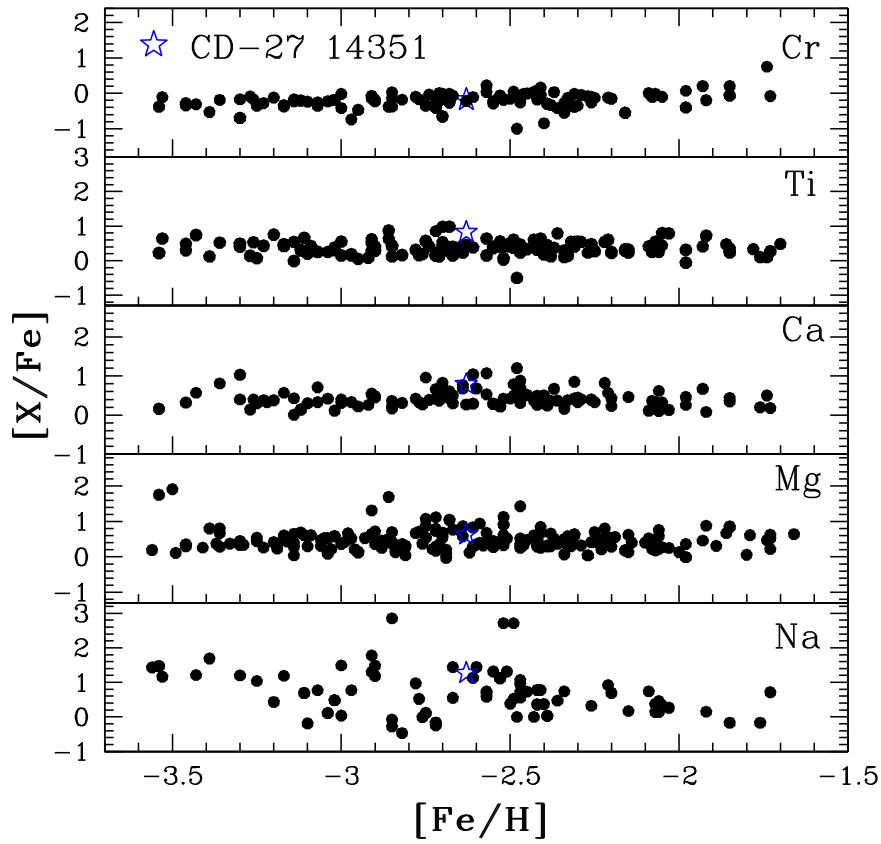


**Figure 8.** Comparison of the observed light-element abundances of CD-27 14351 (indicated by a star symbol) with their counterparts in CEMP stars available in the literature (i.e., Goswami et al. 2006, 2016; Goswami & Aoki 2010; Masseron et al. 2010, Allen et al. 2012).

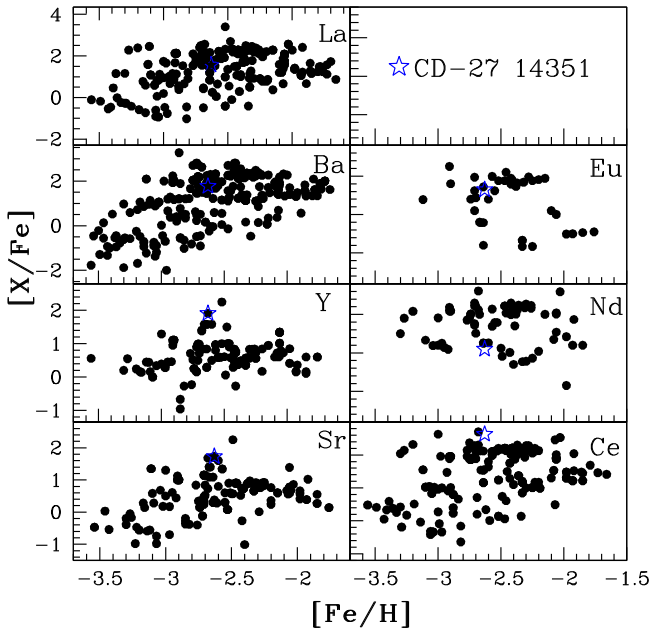


**Figure 9.** Comparison of the observed heavy-element abundances in CD-27 14351 (indicated by a star symbol) with their counterparts in CEMP stars available in the literature (i.e., Goswami et al. 2006, 2016; Goswami & Aoki 2010; Masseron et al. 2010, Allen et al. 2012).

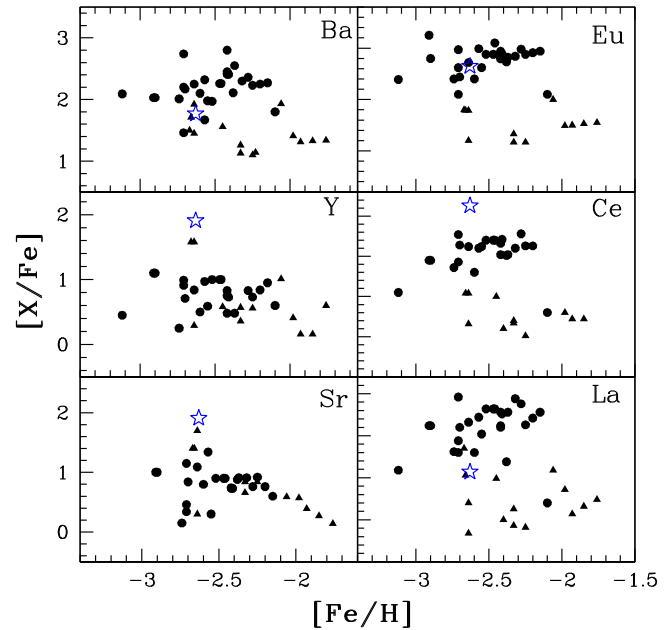


**Figure 10.** Comparison of the observed heavy-element abundances in CD-27 14351 (indicated by a star symbol) with values from other CEMP-r/s (solid circle) and CEMP-s stars (solid triangle) from Jonsell et al. (2006).

estimated  $[La/Ce] = -1.06$  would, therefore, imply the reaction  $^{13}C(\alpha,n)^{16}O$  to be the main source of neutrons. Estimated  $[Ba/Eu] (= 0.12)$  indicates that the object can be

placed in the CEMP-r/s group. Although the binarity among CEMP-s stars is well known, there are a very few studies (e.g., Abate et al. 2016) focused on the orbital properties of CEMP-r/

s stars. In spite of several efforts in the literature, the origin of CEMP-r/s stars still remains far from being clearly understood. However, in future, it would be worthwhile to investigate if the observed abundance pattern in CD-27 14351 could arise from nucleosynthesis of the *i*-process. Our observational results are expected to help constrain theoretical modeling by providing insight and better understanding of the origin of such objects.

A.G., the PI of the HCT observing proposal, and D.K. would like to thank the staff at IAO and at the remote control station at CREST, Hosakote, for assistance during the observations. This work made use of the SIMBAD astronomical database, operated at CDS, Strasbourg, France, and the NASA ADS, USA. Funding from the DST project SB/S2/HEP-010/2013 is gratefully acknowledged. This work was partly supported by the European Union FP7 programme through ERC grant No. 320360.

## REFERENCES

- Abate, C., Stancliffe, R. J., & Liu, Z.-W. 2016, *A&A*, **587**, 50
- Allen, D. M., Ryan, S. G., Rossi, S., Beers, T. C., & Tsangarides, S. A. 2012, *A&A*, **548**, 34
- Alonso, A., Arribas, S., & Martinez-Roger, C. 1999, *A&AS*, **140**, 261
- Alonso, A., Arribas, S., & Martinez-Roger, C. 2001, *A&A*, **376**, 1039
- Andersen, T., Poulsen, O., Ramanujam, P. S., & Petrakiev Petkov, A. 1975, *SoPh*, **44**, 257
- Anderson, E. M., Zilitis, V. A., & Sorokina, E. S. 1967, *OptSp*, **23**, 102
- Aoki, W., Beers, T. C., Christlieb, N., et al. 2007, *ApJ*, **655**, 492
- Aoki, W., Beers, T. C., Sivarani, T., et al. 2008, *ApJ*, **678**, 135
- Aoki, W., Norris, J. E., Ryan, S. G., Beers, T. C., & Ando, H. 2002a, *ApJ*, **567**, 1166
- Aoki, W., Norris, J. E., Ryan, S. G., Beers, T. C., & Ando, H. 2002b, *ApJL*, **576**, L141
- Asplund, M., Grevesse, N., Sauval, J. A., & Scott, P. 2009, *ARA&A*, **47**, 481
- Barbuy, B., Spite, M., Spite, F., et al. 2005, *A&A*, **429**, 1031
- Baumüller, D., & Gehren, T. 1997, *A&A*, **325**, 1088
- Beers, T. C., & Christlieb, N. 2005, *ARA&A*, **43**, 531
- Biemont, E., Karner, C., Meyer, G., Traeger, F., & Zu Putlitz, G. 1982, *A&A*, **107**, 166
- Bridges, J. M., & Kornblith, R. L. 1974, *ApJ*, **192**, 793
- Brooke, J. S. A., Bernath, P. F., Schmidt, T. W., & Bacskay, G. B. 2013, *JQSRT*, **124**, 11
- Corliss, C. H., & Bozman, W. R. 1962a, NBS Monograph 53
- Corliss, C. H., & Bozman, W. R. 1962b, NBS Monograph 53. adjusted
- Cowley, C. R., & Corliss, C. H. 1983, *MNRAS*, **203**, 651
- Führ, J. R., Martin, G. A., & Wiese, W. L. 1988, *JPCRD*, **17**, 4
- Gallino, R., Arlandini, C., Busso, M., et al. 1998, *ApJ*, **497**, 388
- Goriely, S., & Mowlavi, N. 2000, *A&A*, **362**, 599
- Goriely, S., & Siess, L. 2005, *IAU*, **228**, 451
- Goswami, A. 2005, *MNRAS*, **359**, 531
- Goswami, A., & Aoki, W. 2010, *MNRAS*, **404**, 253
- Goswami, A., Aoki, W., Beers, T. C., et al. 2006, *MNRAS*, **372**, 343
- Goswami, A., Aoki, W., & Karinkuzhi, D. 2016, *MNRAS*, **455**, 402
- Hampel, M., Stancliffe, R., Lugaro, M., & Meyer, B. S. 2016, *ApJ*, **831**, 171
- Hannaford, P., Lowe, R. M., Grevesse, N., Biemont, E., & Whaling, W. 1982, *ApJ*, **261**, 736
- Johnson, J. A. 2002, *ApJS*, **139**, 219
- Jonsell, K., Barklem, P. S., Gustafsson, B., et al. 2006, *A&A*, **451**, 651
- Kurucz, R. L. 1988, in *Trans. IAU, XXB*, ed. M. McNally (Dordrecht: Kluwer), 168
- Kurucz, R. L., & Peytremann, E. 1975, *SAOSR*, **362**, 1
- Laughlin, C., & Victor, G. A. 1974, *ApJ*, **192**, 551
- Lincke, R., & Ziegenbein, G. 1971, *ZPhy*, **241**, 369
- Martin, G. A., Führ, J. R., & Wiese, W. L. 1988, *JPCRD*, **17**, 3
- Masseron, T., Johnson, J. A., Plez, B., et al. 2010, *A&A*, **509**, A93
- Masseron, T., Plez, B., Van Eck, S., et al. 2014, *A&A*, **571**, A47
- McEachran, R. P., & Cohen, M. 1971, *JQSRT*, **11**, 1819
- McWilliam, A. 1998, *AJ*, **115**, 1640
- Meggers, W. F., Corliss, C. H., & Scribner, B. F. 1975, NBS Monograph, 145
- Miles, B. M., & Wiese, W. L. 1969, NBS Tech. Note, 474
- Nomoto, K., Wanajo, S., Iwamoto, N., & Ishimaru, Y. 2004, in *Proc. 12th Workshop on Nuclear Astrophysics*, ed. E. Müller & H. T. Janka (Garching: MPA), 123
- Qian, Y. Z., & Wasserburg, G. J. 2003, *ApJ*, **588**, 1099
- Ram, R. S., Brooke James, S. A., Bernath, P. F., Sneden, C., & Lucatello, S. 2014, *ApJS*, **211**, 5
- Sneden, C. 1973, PhD thesis, Univ. Texas at Austin
- Sneden, C., Lucatello, S., Ram, R. S., Brooke, J. S. A., & Bernath, P. F. 2014, *ApJS*, **214**, 26
- Wanajo, S., Nomoto, K., Iwamoto, N., Ishimaru, Y., & Beers, T. C. 2006, *ApJ*, **636**, 842
- Ward, L., Vogel, O., Arnesen, A., Hallin, R., & Wannstrom, A. 1985, *PhysS*, **31**, 162
- Worley, C. C., Hill, V., Sobeck, J., & Carretta, E. 2013, *A&A*, **553**, A47
- Zijlstra, A. A. 2004, *MNRAS*, **348**, L23